Vol.23, No.4, PP.87-97 P-ISSN: 2070-4003 E-ISSN: 2664-5548

# **Effect of Magnetic Field on Plasma Engines**

# Hayder Ridha Ali<sup>1,2\*</sup> and Waleed Ibrahim Yaseen<sup>1</sup>

<sup>1</sup>Department of Astronomy and Space, College of Science, University of Baghdad, Baghdad, Iraq <sup>2</sup>Department of Physics, College of Science, University of Kerbala, Karbala, Iraq <sup>a\*</sup>Corresponding author: <a href="hayder.r@uokerbala.edu.iq">hayder.r@uokerbala.edu.iq</a>

### **Abstract**

Ion engines, also known as plasma engines, are a cutting-edge technology for space propulsion that is continually evolving. In this work, a static magnetic field is used in a cylindrical engine placed inside a vacuum chamber at 0.2 mbar, with argon gas, an applied voltage of 5 kV, and an engine power supply of 25-100 watt. The shape and intensity of the magnetic field determine the ion thruster's discharge performance. A cylindrical ion engine was constructed with dimensions of 5, 5.5, and 0.7 cm in length, width, and thickness, respectively. The coil of the ion engine generates a static magnetic field of 9 and 25 mT. This system was used to study the effect of the magnetic field on the ionization rate and plasma distribution. The results showed that the cylindrical magnetic field confined the energetic electrons primarily near the centre of the engine and resulted in an increased ionization rate in this region. The Langmuir probe is used to diagnose plasma parameters, including temperature and density, with and without a magnetic field. The electron density in the centre of the ion engine increased in the presence of the magnetic field 2-6x10<sup>19</sup> m<sup>-3</sup>, while the electron temperature decreased 2-4 eV. The use of a magnetic field reduces the energy consumption of the ion engine and the energy expended to generate plasma, making it suitable for spacecraft.

#### Article Info.

### **Keywords:**

Plasma Engine, Electric Propulsion, Confine Magnetic Field, Langmuir Probe, Plasma Parameters.

### **Article history:**

Received: Jun. 21, 2025 Revised: Oct. 19, 2025 Accepted:Nov. 14, 2025 Published:Dec. 01,2025

### 1. Introduction

Thrusters are a vital mechanism in any form of starship, and scientists are always seeking novel schemes, mechanics, and principles to improve the proficiency of space propulsion. However, contemporary technological breakthroughs need the development of new engines. Thrusters based on thermodynamic principles of mass acceleration may be difficult to generate sufficient ejection velocity, which is why electric propulsion methods to accelerate mass in the shape of plasma have piqued the curiosity of researchers and engineers worldwide. Electric accelerators and dischargers can generate a wide range of plasmas for a number of purposes, including DBD plasma [1], plasma cleaning [2], manufactured mirrors by plasma magnetron [3], surface modification [4]. When utilized as electric propulsion thrusters, they may be relatively compact, making them appropriate for use in CubeSats and small spacecraft [5]. Alternatively, these engines might be massive and powerful enough to transport big spacecraft on short trips to Mars and other distant planets, providing a possible alternative to existing systems that generate actual high specific impulses [6]. Electric propulsion systems use electric current arc discharges, which are among some of the best promising solutions for high thrust systems able to power massive spacecraft required for large-scale surveys of distant planets [7,8]. Because these systems demand a lot of energy, their progress has been hampered greatly due to a lack of appropriate power systems that can be installed aboard spacecraft. Recent advancements in extremely efficient solar cells and other power sources (particularly creating tiny fusion systems appropriate for space requests) have reignited interest in powerful arc-based techniques [6].

In Hall thrusters, the magnetic field intensity is adjusted to magnetize electrons but leave ions alone. The magnetic field alters the plasma characteristics of the channel by preventing electrons from crossing it. In particular, experimental and computational studies have highlighted the role of the magnetic field setup, or the combination of field structure and channel geometry, in the destiny of deteriorated materials [9]. As a result, there has been a current surge of attention in non-standard topologies, which have the potential to significantly reduce erosion rates [10].

The concept of electric propulsion (EP), defined as the usage of an electric power basis to accelerate a propellant and produce thrust in space, was first offered by Konstantin Tsiolkovsky at the turn of the century, followed by Robert Goddard [11]. Electric propulsion has exceptional thrust efficacy and effective velocities that are orders of magnitude higher than characteristic chemical systems, permitting a significant decrease in propellant required to accomplish a mission. The physics and modeling of hall thrusters are thoroughly described in [12, 13].

In this work, we calculated plasma parameters in the absence and presence of a static magnetic field of 9 and 25 mT in a cylindrical engine designed inside a vacuum chamber under a pressure of 0.2 mbar. In all cases, an applied voltage of 5 kV was applied for different values of energy power. The shape and strength of the magnetic field determine the discharge performance of the ion thruster. This system was used to study the effect of the magnetic field on the ionization rate and plasma distribution, which affect the thrust of the ion thruster.

### 2. Plasma Parameters

The term plasma refers to a wide range of macroscopically neutral materials, which include many interacting free electrons and ionized atoms or molecules. However, not all media containing charged particles are classified as plasmas [14]. To exhibit plasma behavior, a set of interacting, charged, and neutral particles must meet certain properties, or plasma criteria. The properties of the plasma formed in this study will be determined by calculating the plasma parameters in the following paragraphs, using voltage and current plots calculated using a single Langmuir probe.

# 2.1. I-V Characteristics of Langmuir Probe

The current and voltage properties of a Langmuir probe are illustrated in Fig. 1. Here, can be see the float potential, which occurs when the ionic current equals the probe's electron current, i.e., the current is zero. There is also the plasma voltage, which is the voltage at which the probe potential equals the plasma potential. I-V is divided into three areas. A negative probe voltage repels electrons while attracting and collecting positive ions. This is known as the ion-saturation area. The probe attracts the most energetic electrons in the area between the plasma and floating potentials, but repels lower-energy electrons. This area is called the electron-retardation region. In the electron-saturation area, the probe is positive in relation to the plasma potential, effectively repelling ions and collecting only electrons [15,16].

# 2.2. Electron Temperature

One of the important parameters in the plasma is the electronic temperature, which can be calculated in several ways. One of the important methods that diagnoses the electronic temperature locally and at a specific point is the Langmuir probe method. When inserting the sensor inside the plasma, an electronic current or the ionic current is pulled

according to the vulnerable tool. Fig. 1 shows the relationship between the current and the voltage of the Langmuir constellation, which shows the stream of electrons and ions.

When drawing the current with the probe voltage, the I-V characteristic can be obtained. In the area of electronic current saturation, the electron temperature ( $T_e$ ) was calculated from the slope of the semi logarithmic plot and the temperature is measured in electron volts [17-20]:

$$KT_e = \frac{1}{slope} \tag{1}$$

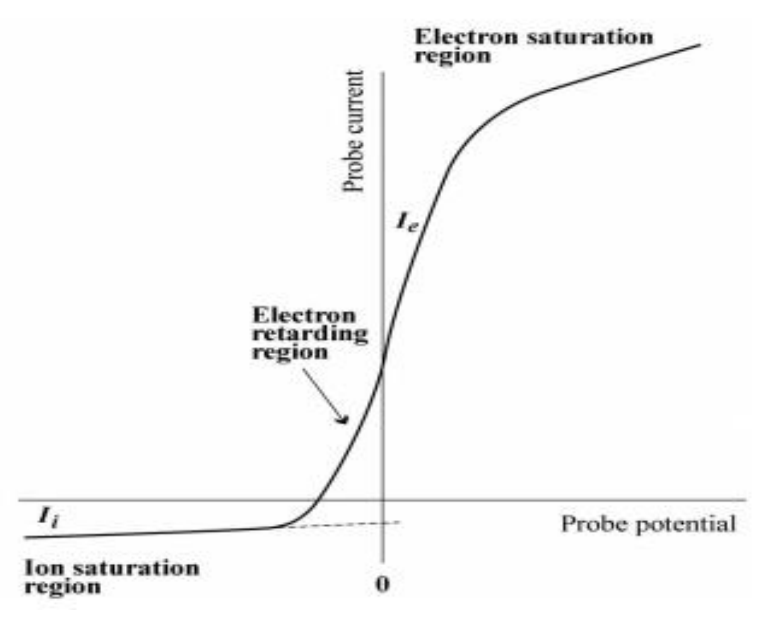


Figure 1: Langmuir probe I-V curve [21].

### 2.3. Electron Density

Another important parameter of plasma is the electronic density that gives a vision of the plasma ionization rate, which can be calculated from measuring the electronic saturation current and the ion saturation current through the curves of the relationship between the current and the voltage of the Langmuir probe. In the first region, as in the form, the probe effort is less than the floating voltage, and given the high concentration of ions in this region, the current is small and negative. From this, the ionic density in the plasma can be determined. As for the second area, when the voltage probe is between the floating voltage and the plasma voltage. Where the electrons are attracted due to the positive effort of the probe, and an electronic cloud is formed around the probe and becomes negative and in turn attracts positive ions and the process continues to reach a state of balance from the floating effort. In the third area, the excessive positive voltage increases and becomes higher than the plasma voltage. As a result, the electron accelerates and the saturation electron increases. The electronic density can be calculated [22-24]:

$$n_e = \frac{I_{es}}{eA_p} \sqrt{\frac{2\pi m}{KT_e}}$$
 (2)

where  $I_{es}$  is the electron saturation current, m is the mass of the electron and  $A_p$  is the surface area of the probe [23]:

$$A_p = \frac{\pi D^2}{4} + \pi Dh \tag{3}$$

Where D is the diameter and h is the length of the wire probe.

A Langmuir probe with a large area can be used to better measure the ion density [25].

# 2.4. Debye Length

The Debye radius is an important parameter for the plasma that can be calculated for a full diagnosis. For the plasma used and represents the Debye radius, or the so called Debye shield, is the response of the charged particles that are largely charged with the effects of the external electrical fields [23]. It depends on the electron density of the plasma and the degree of electron thermal as in the relationship [26-32]:

$$\lambda_D = \sqrt{\frac{\varepsilon_o K T_e}{n_e e^2}} \tag{4}$$

where e electron charge,  $C_0$  permittivity of free space, and K is represented Boltzmann's constant.

Length of Debye must be actual tiny when equalled with the system element.  $\lambda_D << L$  is the first condition for plasma where L is the length system [23,33,34].

### 2.5. Plasma Parameter

The shielding effect can simply be observed when the Debye sphere includes a significant number of electrons. Because of the exponential decline in the potential, it can be determined that the shielding is produced by electrons in the Debye sphere, and their number is certain by [26,27,31,32]:

$$N_D = \frac{4\pi n_e \lambda_D^3}{3} \tag{5}$$

# 3. Influence of the Magnetic Field on the Plasma Parameters

The magnetic field effects on the plasma density and energy distribution while also having a direct impact on electric field distribution. The behaviour of the plasmas effects beam extraction, thrust, and efficiency [35]. As a result, a hall thruster relies heavily on the magnetic field in the discharge channel. There has previously been much research on the magnetic field. In conventional magnetic field design theory, radial magnetic lenses are utilized to concentrate the ions, and the intensity has a positive gradient [12]. For an acceptable magnetic field figure, the current density must be low [36], the magnetic field at the anode should be almost zero, and the magnetic field incline should be as big as feasible [37, 38].

# 4. Experimental Part

Fig. 2 illustrates the vacuum system, and it consists of chamber made from glass with measurements 20, 30, 0.5 cm width, length, and thickness, respectively, lying on a stainless-steel base. The air is evacuated by two stage rotaries to reduce the pressure to  $2x10^{-2}$  mbar. At the same time, we pumped Argon gas through a special opening while maintaining low pressure within the system. A DC power supply with a voltage of up to 5 kV is supplied to the system. In addition, a DC power supply of 100 volts is given to the Langmuir probe, where used tungsten wire for design and construction with a length

of 4 mm and a diameter of 0.4 mm, as shown in Fig. 3. A voltmeter and an ammeter are connected to the system to measure the voltage and current passing through the probe.

In this work, the current and voltage generated by Argon gas ionization inside a vacuum chamber model of ion engines can be calculated using a Langmuir probe to characterise the generated plasma. To simulate the operating conditions of the plasma ion engine, the quantities were taken at a pressure of  $2x10^{-2}$  mbar at variable powers from a high-voltage power supply ranging from 25 to 100 W, mounted between the ion thruster electrodes in the engine.

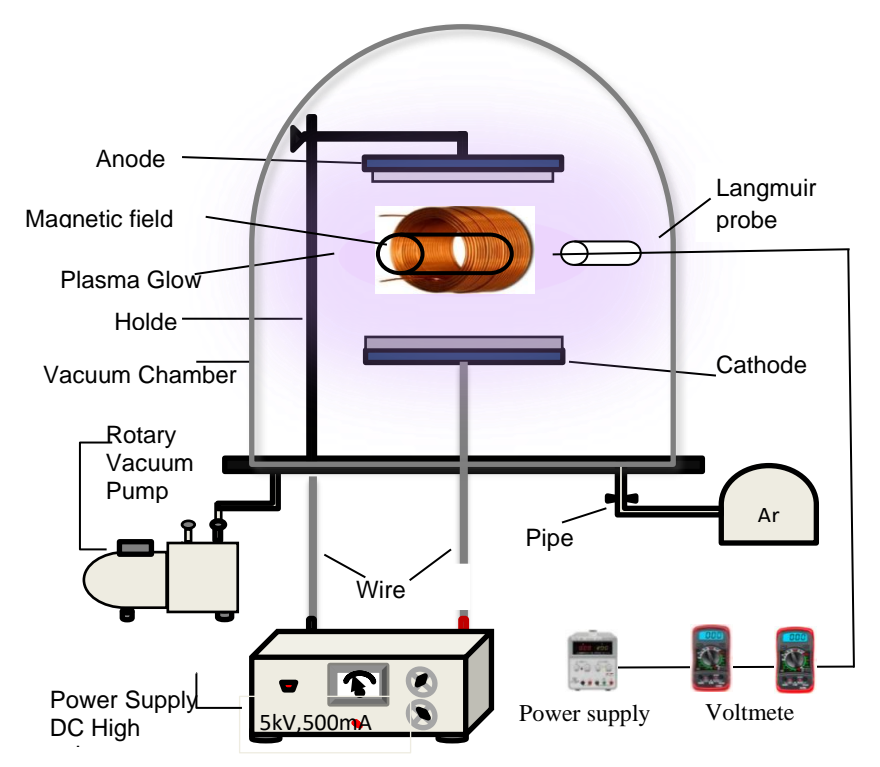


Figure 2: The compensation of the system.

A Langmuir probe was used to characterise the plasma generated inside the engine models designed in this work, and the current and voltage of the power supply were calculated during the gas ionization process inside the vacuum chamber. These experiments were conducted to simulate the operating conditions of ion engines in a real environment. An operating pressure of approximately  $2x10^{-2}$  mbar was used inside the vacuum chamber, and variable values of the power supply were applied to generate plasma inside the engines inside the vacuum chamber. The power values ranged from 25 to 100 W.



Figure 3: The Langmuir probe that made of tungsten wire.

An external magnetic field is applied to the cylindrical ion engine by the external magnetic coil located around the discharge chamber, with dimensions 5, 5.5 and 0.7 cm in length, width and thickness respectively with a wire diameter of 1 mm and have 385 turns, as shown in Fig. 2. A Tesla meter was used to measure the magnetic field strength of the coil used in this work. The diameter of the cylindrical coil was divided into 7 regions as shown in Fig. 4. According to the coil design, there is a maximum value of magnetic field strength at a distance of 2 cm, where the magnetic field flux is very high in this region, leading to an increase in the number of electron density of the plasma in the center of the cylindrical coil and the ion engine due to the increase in the ionization rate and reduced collisions between electrons and the engine walls to conserve electron energy.

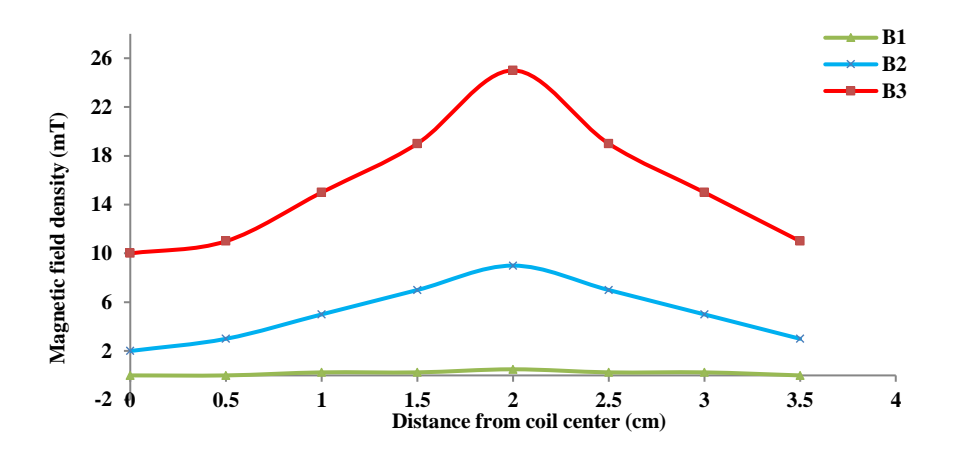


Figure 4: Magnetic field density with the distance of the cylindrical coil.

The plasma appears as a luminous cylindrical shape along the axis of the engine, as shown in Fig. 5. Two values of the magnetic field (9 and 25) mT were used. The magnetic field strength was plotted with the radial distance of the cylindrical coil, and three curves representing the magnetic field strength appeared as shown in Fig. 4.

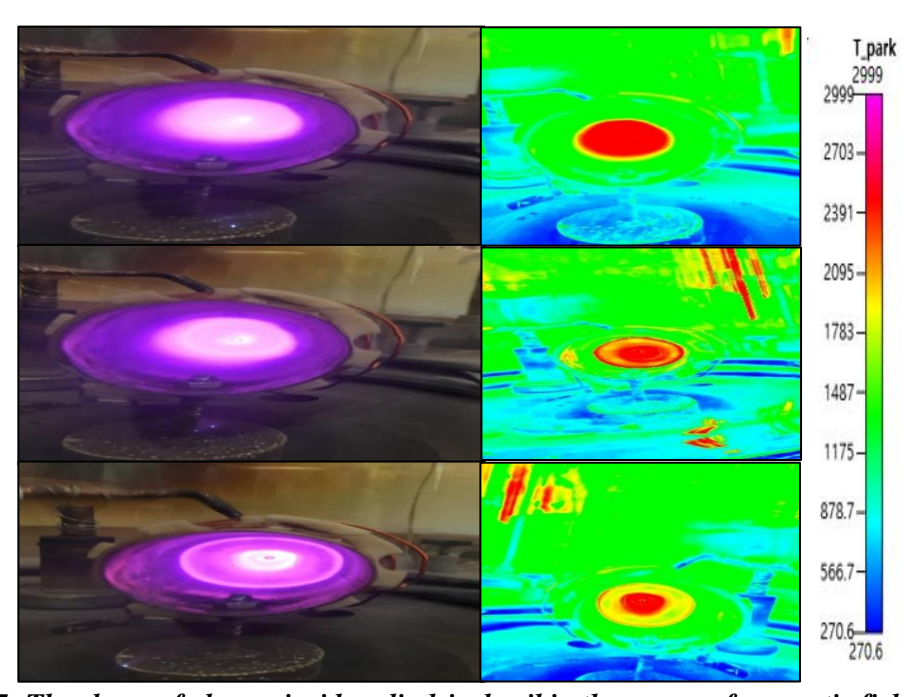


Figure 5: The shape of plasma inside cylindrical coil in three case of magnetic field density.

The relationship between current and voltage has been calculated for all ion thrusters. By plotting this relationship, the electron temperature can be calculated from the reciprocal of the slope of the tangent line at the electron saturation point using Eq. (1). By calculating the effective area of the Langmuir probe using Eq. (2), the plasma electron density can be calculated for ion thruster models. In this work, the Debye radius  $\lambda_D$ , and the number of ionized atoms within the Debye radius  $N_D$  with varying the supplied power were calculated using Eqs. (4 and 5).

### 5. Results and Discussion

Electron current was calculated by use of a Langmuir probe with applied positive and negative potential to collect electrons and ions for all cases. Then plotted currents as a function of the applied voltage to determine the (I-V) characteristics as shown in Fig. 6. And calculating the slope for each curve to determine the temperature of the electron  $T_e$  with Eq. (1). After taking the logarithm of the positive current and plotting it with the applied voltage to estimate the electron saturation current  $I_{es}$  to use it to calculate the density of electrons by Eq. 2. After that, we calculated the plasma parameters for each of the Debye length  $\lambda_D$ , the number of electrons inside the Debye length  $N_D$  by using Eqs. (4 and 5).

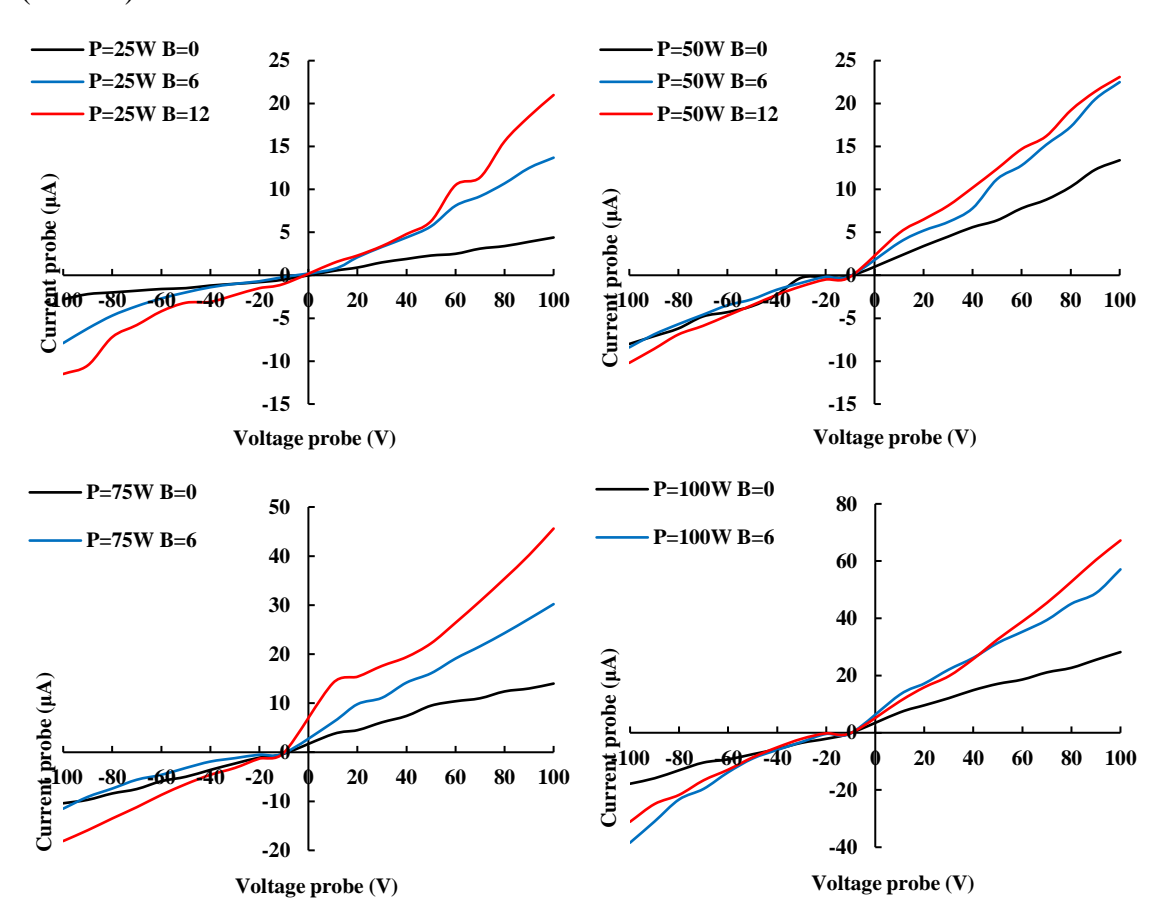


Figure 6: The I-V plot for engine with different magnetic field.

The electron temperature decreases with an increased energy of the power supply, which may be due to an increase in electron collision frequency with plasma species. This result agrees with [30,39,40]. And the temperature curves are shifted to lower values with the presence of a magnetic field. As shown in Fig. 7. This shifted due to enclosing the plasma in a small area in the center of the ion thruster, and the collision frequency

increased between plasma species, and plasma moved away from a wall of the ion thruster.

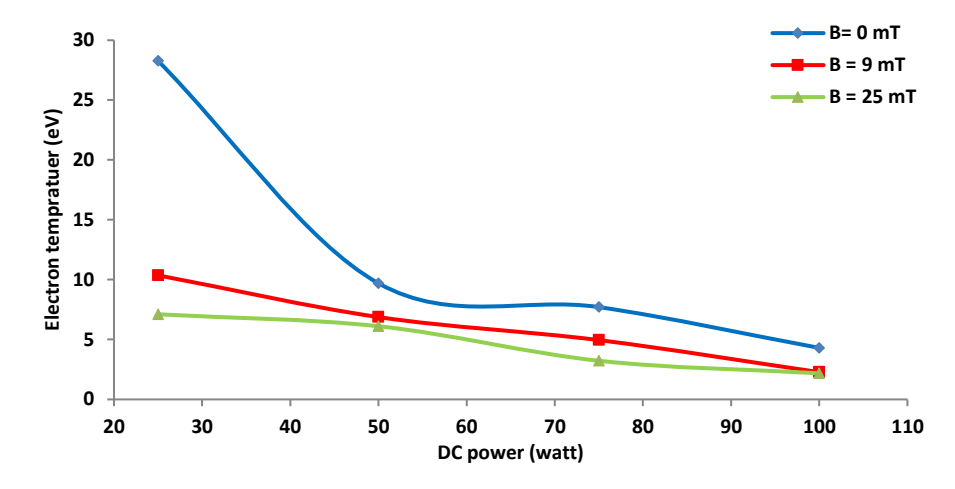


Figure 7: Temperature of electron vs. DC power for different magnetic fields.

When the power of the power supply increases, the electron density rises, as shown in Fig. 8.

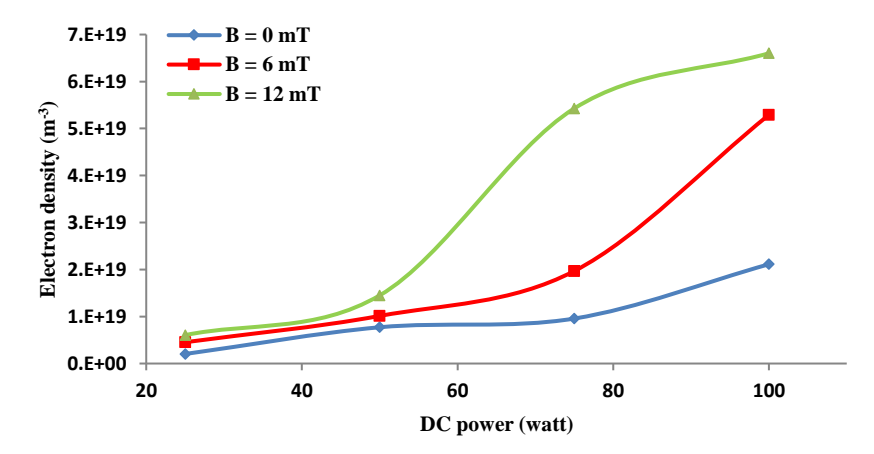


Figure 8: Electron density vs. DC power for different magnetic fields.

When energy increases, the plasma ionization increases due to the increased intensity of the electric field inside the ion thruster. This agrees with [30,39,40]. In the case of the presence of a magnetic field, the electron density curves are shifted to high values because plasma is confined by a magnetic field in the centre of the ion engine, therefore, collision and ionization will increase. Since the Debye radius depends on the temperature of the electron directly and the density of the electrones inversely, it decreases with the increase in the power due to the increased density of the electrons. It agrees with [30,40,41]. And the Debye radius reduced with an increased magnetic field due to confining the ions in a small area. It is shown in Fig. 9.

The difference in the behavior of the Debye length curve in the absence of a magnetic field may be due to the presence of a thermal effect versus a density effect, which leads to an overlap between the effect of DC power on electron temperature and its effect on electron density, with the temperature effect initially dominant. Therefore, this behavior may indicate that the initial increase in DC power primarily leads to a larger increase in electron temperature than in electron density, up to a certain point after which the effect of the increased density becomes dominant, leading to the curve's behavior

matching that of the other curves. All the results which were obtained are illustrated in Table 1.

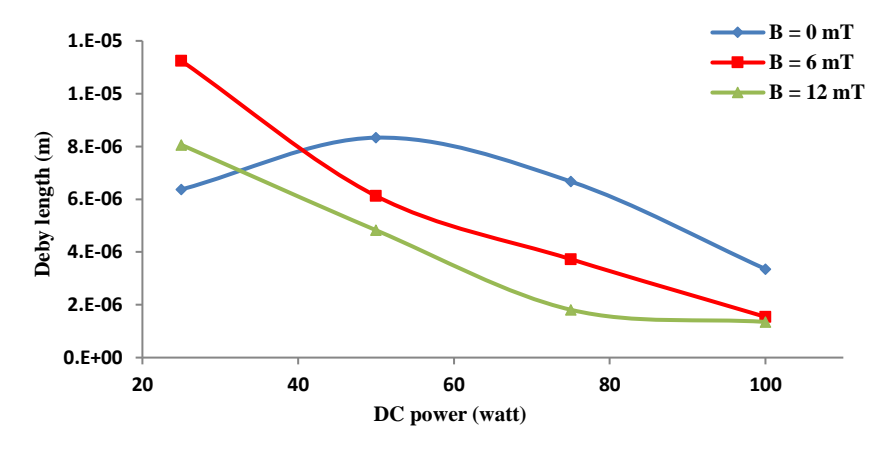


Figure 9: Debye length vs. DC power for different magnetic fields.

Table 1: The plasma parameters with and without a magnetic field.					
B (mT)	P (W)	T <sub>e</sub> (eV)	n <sub>e</sub> (m <sup>-3</sup> )	λ <sub>D</sub> (m)	N <sub>D</sub>
0	25	28.2776	2.03E+18	6.4E-06	2.20E+03
	50	9.69895	7.72E+18	8.3E-06	1.87E+04
	75	7.70848	9.57E+18	6.7E-06	1.19E+04
	100	4.3024	2.11E+19	3.4E-06	3.34E+03
9	25	10.3634	4.53E+18	1.1E-05	2.70E+04
	50	6.875	1.01E+19	6.1E-06	9.75E+03
	75	4.95304	1.97E+19	3.7E-06	4.28E+03
	100	2.27582	5.29E+19	1.5E-06	8.12E+02
25	25	7.10857	6.04E+18	8.1E-06	1.33E+04
	50	6.11257	1.45E+19	4.8E-06	6.83E+03
	75	3.22554	5.43E+19	1.8E-06	1.35E+03
	100	2 18093	6.60F±19	1 4F-06	6.82F+02

Table 1: The plasma parameters with and without a magnetic field.

### 6. Conclusions

The experimental results reveal several significant findings regarding the effects of magnetic fields on the operating parameters of the cylindrical ion engine under investigation. Using laboratory measurements taken during the engine's discharge process across a range of applied magnetics flux densities, it was unequivocally established that, under fixed geometric and operational parameters, the magnetic field generated by the cylindrical coil significantly improves the engine's efficiency. This enhancement is related to the B field's confinement of electrons towards the engine's central axis, a phenomenon known as the Lorentz force. Increased electron confinement increases the chance of inelastic electron-neutral atom collisions, which boosts the ionization rate at the discharge chamber's core. This method results in a significant increase in plasma electron density. Furthermore, the magnetic field application was discovered to minimize the power consumption of the ion engine, decreasing the needed operating potential or power supply. This feature is handy for spaceship propulsion systems, where maximizing thrust-to-power ratio and minimizing energy consumption are essential design goals.

### **Conflicts of Interest**

The authors declare there is no conflict of interest.

### References

- 1. A. K. Abd and Q. A. Abbas, Iraqi J. Sci. 64(6), 2867 (2023). https://doi.org/10.24996/ijs.2023.64.6.17.
- W. I. Yaseen and D. A. Al-Shakarchi, Iraqi J. Sci. 65(6), 3484 (2024). https://doi.org/10.24996/ijs.2024.65.6.40.
- 3. H. A. Sadeq and W. I. Yaseen, Iraqi J. Sci. **63**(5), 2297 (2022). https://doi.org/10.24996/ijs.2022.63.5.39.
- 4. M. V. Jacob, R. S. Rawat, B. Ouyang, K. Bazaka, D. S. Kumar, D. Taguchi, M. Iwamoto, R. Neupane, and O. K. Varghese, Nano letters 15(9), 5702 (2015). <a href="https://doi.org/10.1021/acs.nanolett.5b01363">https://doi.org/10.1021/acs.nanolett.5b01363</a>.
- 5. I. Levchenko, K. Bazaka, Y. Ding, Y. Raitses, S. Mazouffre, T. Henning, P. J. Klar, S. Shinohara, J. Schein, and L. Garrigues, Appl.Phy.Rev. 5 (1), 1 (2018). <a href="https://doi.org/10.1063/1.5007734">https://doi.org/10.1063/1.5007734</a>.
- 6. O. Baranov, I. Levchenko, S. Xu, X. Wang, H. Zhou, and K. Bazaka, Reviews of Modern Plasma Physics **3**(7), 1 (2019). <a href="https://doi.org/10.1007/s41614-019-0023-3">https://doi.org/10.1007/s41614-019-0023-3</a>.
- 7. A. Kitaeva, H. Tang, B. Wang, and T. Andreussi, Vacuum **159**, 324 (2019). <a href="https://doi.org/10.1016/j.vacuum.2018.10.046">https://doi.org/10.1016/j.vacuum.2018.10.046</a>.
- 8. I. Levchenko, O. Baranov, D. Pedrini, C. Riccardi, H. E. Roman, S. Xu, D. Lev, and K. Bazaka, Appl. Sci. **12**(21), 11143 (2022). <a href="https://doi.org/10.3390/app122111143">https://doi.org/10.3390/app122111143</a>.
- 9. I. G. Mikellides, R. R. Hofer, I. Katz, and D. M. Goebel, J. App. Phy. **116**(5), 053302 (2014). http://doi.org/10.1063/1.4892160.
- 10. J. Cruz, Y. Wu, J. E. Candelo-Becerra, J. C. Vásquez, and J. M. Guerrero, CSEE Journal of Power and Energy Systems **10**(2), 448 (2024). <a href="https://doi.org/10.17775/CSEEJPES.2022.07980">https://doi.org/10.17775/CSEEJPES.2022.07980</a>.
- 11. E. Y. Choueiri, Journal of Propulsion and Power **20**(2), 193 (2004). https://doi.org/10.2514/1.9245.
- 12. D. M. Goebel, I. Katz, and I. G. Mikellides, *Fundamentals of electric propulsion*. John Wiley & Sons, (2023).
- 13. J.-P. Boeuf, J. App. Phy. 121, 011101 (2017). http://doi.org/10.1063/1.4972269.
- 14. R. Eduard Vardges, *In* Selected Topics in Plasma Physics, S. Sukhmander Intech Open, Rijeka, (2020). https://doi.org/10.5772/intechopen.91222.
- F. Magnus and J. Gudmundsson, Review of Scientific Instruments 79, 073503 (2008). https://doi.org/10.1063/1.2956970.
- 16. S. Bhattarai, World J. Appl.Phys. 2(2), 50 (2017). https://doi.org/10.11648/j.wjap.20170202.13.
- 17. T. A. Hameed and S. J. Kadhem, Iraqi J. Sci. **60**(12), 2649 (2019). https://doi.org/10.24996/ijs.2019.60.12.14.
- 18. S. H. Abd Muslim, *In* Proceedings of the Mustansiriyah International Conference on Applied Physics (MICAP-2021) Acta Physica Polonica A, Baghdad, Iraq, 2021, p. 358.
- 19. J.-Q. Li, X.-Y. Xie, Q.-H. Zhang, S.-H. Li, and W.-Q. Lu, Physics of Fluids **34**, 6 (2022). https://doi.org/10.1063/5.0097089.
- 20. L. Conde, *In* Dept. Física. ETSI Aeronáut ngenieros Aeronáuticos Universidad Politécnica de Madrid, Madrid, Spain, (2011), p. 28.
- 21. T. Abe and K.-i. Oyama, *In* An introduction to space instrumentation Terra Pu b., 1st (2013), p. 63, <a href="https://doi.org/10.5047/aisi.010">https://doi.org/10.5047/aisi.010</a>.
- 22. S. Bhattarai and L. N. Mishra, International Journal of Research-GRANTHAALAYAH **5**(4), 228 (2017). <a href="https://doi.org/10.5281/zenodo.571529">https://doi.org/10.5281/zenodo.571529</a>.
- 23. A. A. Hussain, K. A. Aadim, and W. I. Yaseen, Iraqi J. Phys. **13**(27), 76 (2015). https://doi.org/10.30723/ijp.v13i27.266.
- 24. B. M. Schulz, M.Sc., Western Michigan University, (2024).
- 25. M. Pandya, H. Kabariya, S. Karkari, and H. Patel, *In* Nirma University International Conference on Engineering (NUiCONE) IEEE, Ahmedabad, India, 2013, p. 6.
- 26. S. M. Fathi and S. J. Kadhim, Iraqi J. Sci. 63(1), 163 (2022). https://doi.org/10.24996/ijs.2022.63.1.17.
- 27. F. K. Hammoud and K. A. Aadim, Iraqi J. Sci. **63**(4), 1540 (2022). https://doi.org/10.24996/ijs.2022.63.4.14.
- 28. M. F. Hassan and W. I. Yaseen, Iraqi J. Sci. **64**(6), 3194 (2023). https://doi.org/10.24996/ijs.2023.64.6.45.
- 29. J. Chen, H. Geng, W. Meng, N. Yan, J. Hu, and X. Li, AIP Advances **14**(8), (2024). https://doi.org/10.1063/5.0220087.
- 30. A. Shrestha, R. Shrestha, H. Baniya, R. Tyata, D. Subedi, and C. Wong, International Journal of Recent Research and Review VII, 2, 9 (2014). <a href="https://doi.org/10.13140/2.1.2159.1685">https://doi.org/10.13140/2.1.2159.1685</a>.
- 31. H. Q. Farag and J. K. Saba, Iraqi J. Phys. **20**(4), 45 (2022). https://doi.org/10.30723/ijp.v20i4.1056.
- 32. A. A. Temur and A. F. Ahmed, Iraqi J. Sci. **63**(7), 3225 (2022). https://doi.org/10.24996/ijs.2022.63.7.41.
- 33. K. Dobbyn, M.Sc., Dublin City University, (2000).
- 34. H. O. Hussein and Waleed Ibrahim Yaseen, Iraqi J. Sci. **65**(5), 2925 (2024). <a href="https://doi.org/10.24996/ijs.2024.65.5.43">https://doi.org/10.24996/ijs.2024.65.5.43</a>.

- 35. Y. Izawa, K. Suzuki, K. Takahashi, and A. Ando, *In* Proceedings of the 12th Asia Pacific Physics Conference (APPC12) Japan, 2014.
- 36. R. R. Hofer, R. S. Jankovsky, and A. D. Gallimore, Journal of Propulsion and Power **22**(4), 721 (2006). https://doi.org/10.2514/1.15952.
- 37. K. Xie, F. Tian, L. Fuwen, Q. Xia, and N. Wang, Plasma Sci. Technol. **22**(9), 094011 (2020). <a href="https://doi.org/10.1088/2058-6272/ab9bf9">https://doi.org/10.1088/2058-6272/ab9bf9</a>.
- 38. L. Yang, P. Wang, and T. Wang, Front. Mater. **10**, 1279039 (2023). <a href="https://doi.org/10.3389/fmats.2023.1150802">https://doi.org/10.3389/fmats.2023.1150802</a>.
- 39. M. Quitzau and H. Kersten, Eur. Phys. J.D, **66**(2), 47 (2012). <a href="https://doi.org/10.1140/epjd/e2012-20216-5">https://doi.org/10.1140/epjd/e2012-20216-5</a>.
- 40. A. M. Ahadi, T. Trottenberg, S. Rehders, T. Strunskus, H. Kersten, and F. Faupel, Phys. Plasmas **22**(8), 083513 (2015). https://doi.org/10.1063/1.4929788.
- 41. M. K. Jassim, Ibn AL-Haitham Journal For Pure and Applied Sciences **32**(2), 9 (2019). https://doi.org/10.30526/32.2.2126.

# تأثير المجال المغناطيسى على محركات البلازما

حيدر رضا علي  $^{2,1}$  وو ليد ابر اهيم ياسين  $^{1}$  تقسم الفلك والفضاء، كلية العلوم، جامعة بغداد، بغداد، العراق  $^{2}$  قسم الفيز باء، كلبة العلوم، جامعة كر بلاء، كر بلاء، العراق

#### الخلاصة

تعتبر محركات الأيونات، والمعروفة أيضًا بمحركات البلازما، هي تقنية متطورة الدفع الفضائي تتطور باستمرار. في هذا العمل، يُستخدم مجال مغناطيسي ثابت في محرك أسطواني موضوع داخل غرفة تفريغ عند 0.2 ملي بار، مع غاز الأرجون، وجهد مطبق 5 كيلو فولت، ومصدر طاقة محرك يتراوح بين 25 و 100 واط. يحدد شكل وشدة المجال المغناطيسي أداء تفريغ الدافع الأيوني. تم بناء محرك أيوني أسطواني بأبعاد 5 و 5.5 و 0.7 سم في الطول والعرض والسمك على التوالي. يولد ملف المحرك الأيوني مجالًا مغناطيسيًا ثابتًا يبلغ 9 و 25 ملي تسلا. استُخدم هذا النظام لدراسة تأثير المجال المغناطيسي على معدل التأين وتوزيع البلازما. أظهرت النتائج أن المجال المغناطيسي الأسطواني حصر الإلكترونات النشطة بشكل أساسي بالقرب من مركز المحرك مما أدى إلى زيادة معدل التأين في هذه المنطقة. يُستخدم مسبار لانجموير لتشخيص معاملات البلازما، بما في ذلك درجة الحرارة والكثافة، سواءً بوجود مجال مغناطيسي أو بدونه. ازدادت كثافة الإلكترونات في مركز محرك الأيونات بوجود مجال مغناطيسي مقداره 10°ء ك-6 متر مكعب، بينما انخفضت درجة حرارة الإلكترونات بمعارف المبدولة لتوليد البلازما، مما بعدام المجال المغناطيسي من استهلاك محرك الأيونات للطاقة والطاقة المبذولة لتوليد البلازما، مما يجعله مناسبًا للمركبات الفضائية.

الكلمات المفتاحيه: محرك البلازما، الدفع الكهربائي، المجال المغناطيسي المحصور، مجس لانكمور، معلمات البلازما.